GLOBAL BIOGEOCHEMICAL CYCLES, VOL. 15, NO. 4, PAGES 767–782, DECEMBER 2001

Estimating net air-sea fluxes from ocean bulk data: Methodology and application to the heat cycle

Manuel Gloor,[1] Nicolas Gruber,[2] Tertia M. C. Hughes,[3] and Jorge L. Sarmiento
Atmospheric and Oceanic Sciences Program, Princeton University, Princeton, New Jersey, USA

Abstract. A novel method to estimate annual mean heat, water, and gas exchange fluxes between the ocean and the atmosphere is proposed that is complementary to the traditional approach based on air-sea gradients and bulk exchange parameterization. The new approach exploits the information on surface exchange fluxes contained in the distribution of temperature, salinity, and dissolved gases in the ocean interior. We use an Ocean General Circulation Model to determine how the distribution in the ocean interior is linked to surface fluxes. We then determine with least squares the surface fluxes that are most compatible with the observations. To establish and test the method, we apply it to ocean temperature data to estimate heat fluxes across the air-sea interface for which a number of climatological estimates exists. We also test the sensitivity of the inversion results to data coverage, differences in ocean transport, variations in the surface flux pattern and a range of spatial resolutions. We find, on the basis of the World Ocean Circulation Experiment (WOCE) data network augmented with selected high-quality pre-WOCE data, that we are able to constrain heat exchange fluxes for 10–15 regions of the ocean, whereby these fluxes nearly balance globally without enforcing a conservation constraint. Our results agree well with heat flux estimates on the basis of bulk exchange parameterization, which generally require constraints to ensure a global net heat flux of zero. We also find that the heat transports implied by our inversely estimated fluxes are in good agreement with a large range of heat transport estimates based on hydrographic data. Increasing the number of regions beyond the 10–15 regions considered here is severely limited because of modeling errors. The inverse method is fairly robust to the modeling of the spatial patterns of the surface fluxes; however, it is quite sensitive to the modeling of ocean transport. The most striking difference between our estimates and the heat flux climatologies is a large heat loss of 0.64 PW to the atmosphere from the Southern Ocean and a large heat gain by the subpolar South Atlantic of 0.56 PW. These results are consistent with the large gain of carbon dioxide called for by *Takahashi et al.* [1999] in his recent analysis of the air-sea flux of carbon dioxide but inconsistent with the large loss of oxygen and carbon dioxide such as those of *Stephens et al.* [1998].

1. Introduction

The most common method to estimate gas exchange between the ocean and the atmosphere is to measure the partial pressure difference at the ocean surface and to apply an exchange coefficient parameterized to summarize all contributing processes [*Liss and Merlivat*, 1986; *Wanninkhof*, 1992; *Watson et al.*, 1991; *Wanninkhof and McGillis*, 1999]. Parameterizations of the gas exchange coefficient have been determined empirically in laboratories, lakes, and in the ocean and have been compared against the global budget of bomb ^{14}C [*Broecker et al.*, 1985, 1995; *Wanninkhof et al.*, 1991; *Wanninkhof and McGillis*, 1999]. One of the most common methods to estimate heat exchange between the ocean and the atmosphere is similarly based on measurements close to the ocean surface and parameterizations of exchange coefficients. The measurements include the temperature and humidity gradients and solar shortwave and terrestrial thermal radiation. Both approaches have a similar problem: the uncertainties introduced by the parameterizations are large [*Takahashi et al.*, 1997; *da Silva et al.*, 1994; *Josey et al.*, 1999]. This problem is illustrated by the fact that the direct application of bulk formulas to estimate the air-sea heat exchange results in large imbalances when integrated over the globe [*Josey et al.*, 1999]. In most studies, this imbalance is removed by allowing for small changes of bulk parameterizations and forcing heat transports toward heat transports derived from hydrographic data [*da Silva et al.*, 1994; *Esbensen and Kushnir*, 1981].

We propose here an alternative inverse approach to estimate annual mean exchange fluxes between the oceans and the atmosphere that uses the information on exchange fluxes contained in the distributions of conserved quantities in the ocean interior. We extract this information from the ocean bulk data by comparing them with model predicted distributions obtained when tracer is released from different regions at the ocean surface and determining the combination of these distributions that reproduce the observations most closely. This approach implictly assumes that the ocean circulation and the sources and sinks of the quantity under investigation have not changed considerably over the last few ocean overturning cycles.

A related "inverse box model" approach has been pursued by *Rintoul and Wunsch* [1991] and *Macdonald and Wunsch* [1996]

[1]Now at Max-Planck Institut für Biogeochemie, Jena, Germany.
[2]Now at Institute of Geophysics and Planetary Physics and Department of Atmospheric Sciences, University of California, Los Angeles, California, USA.
[3]Deceased November 23, 1998.

Paper number 2000GB001301.
0886-6236/01/2000GB001301$12.00

and most recently by *Ganachaud and Wunsch* [2000]. These authors use measurements of temperature, salinity, oxygen, and dissolved nutrients to estimate the ocean circulation. The velocity field is assumed to be in geostrophic balance, and transport by eddies is parameterized as diffusion. Typically, the number of knowns is of the order of thousands, and the number of unknowns is 2–5 times larger than the number of unknowns. A major difference between our method and the method of Rintoul and Wunsch, Macdonald and Wunsch, and Ganachaud and Wunsch is that we employ the simulated transport fields from an Ocean General Circulation Model (OGCM) instead of estimating it directly from the measurements. We are thus not restricted to the assumption of geostrophic flow, and processes like convection are not parameterized as eddy diffusion. A disadvantage of our method, as we will demonstrate, is that it is difficult to take into account formally biases in modeled transport.

Compared to the troposphere, where gradients of gases relax over a timescale of the order of half a year [*Maiss and Levin*, 1994], mixing in the oceans is slow. The estimates for deep water renewal of the oceans, a rough analog of the timescale for interhemispheric exchange in the atmosphere, are of the order of 1000 years [*Stuiver et al.*, 1983]. In contrast to the atmosphere, concentration distributions in the ocean therefore bear information from fluxes several hundreds of years before today. If it is possible to correct for the anthropogenic perturbation and biological transformations of a substance [see *Gruber et al.*, 1996; this issue], it should be possible, in principle, to estimate not only contemporary but also preindustrial steady state exchange fluxes of, for example, carbon.

An additional consequence of the different mixing timescales in the ocean and the atmosphere is that ocean observations from different years may be combined to obtain very large data sets with hundreds of thousands of measurements that extend from the ocean surface to the deep sea. Unlike the atmosphere, inverse modeling of air-sea exchange fluxes is therefore not likely to be hampered by insufficient data coverage (inversions may still be unstable because of the diffusive nature of the ocean circulation). For comparison, continuous measurements of trace substances like CO_2 in the atmosphere are mostly confined to the surface and the number of stations is of the order of 100 only.

The aim of this paper is to provide an overview of the potential and limits of the methodology for future application to the carbon and oxygen cycles. To achieve this goal, we chose as a first step to apply the method to the cycling of heat in the oceans. The heat cycle is particularly suited for our purpose because there are several heat flux and temperature climatologies and because the temperature data coverage of the oceans is good.

The paper first introduces the methodology, then discusses and evaluates the impact of various sources of uncertainty such as deficiencies of transport simulations or data coverage. We then present estimates of model-model inversions, a model ocean climatology inversion, and inversions on the basis of recent temperature observations. Finally, surface heat fluxes obtained by the inversions are discussed and put into perspective with existing estimates obtained with surface flux parameterizations. Similarly, the implied ocean heat transports are compared with estimates based on ocean hydrographic data. We will show that this new methodology results in heat flux estimates that are of similar quality as the most recent heat flux climatologies. This suggests that our approach is suited to be applied to other ocean tracers that are exchanged across the air-sea interface.

2. Method

We directly adapt to the oceans a time-independent inverse scheme originally devised to estimate CO_2 sources and sinks from atmospheric observations [*Bolin and Keeling*, 1963; *Enting and Mansbridge*, 1989; *Keeling et al.*, 1989; *Fan et al.*, 1998]. Our intent is to apply the method to ocean biogeochemical cycles at steady state. The method when applied to dissolved gases takes advantage of the linearity of the tracer transport equation. Note that the transport equation for heat is nonlinear because the velocity field is coupled to temperature. Since a main purpose of the paper is to evaluate the method for application to air-sea exchange of biogeochemically relevant substances, we here treat heat as a passive tracer. The linearity property of the transport equation permits decomposition of an observed tracer distribution into the sum of contributions that result when tracer is released from n different surface regions, such as tracer release restricted to the North Atlantic versus release from the Southern Ocean. To determine these distributions, we impose annually periodic surface fluxes φ_i from each surface region $i = 1,\ldots,n$ of an Ocean General Circulation Model (OGCM) and integrate the OGCM forward in time until the tracer distributions reach a quasi-stationary state. The quasi-stationary state is reached when the annually averaged spatial concentration distribution increases at the same rate throughout the entire ocean. Model transport thus establishes an exact relation between any linear combinations of the imposed surface fluxes $(\lambda_1\varphi_1,\ldots,\lambda_n\varphi_n)$ and the concentration distribution in the ocean interior when referenced to the concentration at a fixed location $\vec{x}_{\mathrm{ref}}$

$$\Delta\vec{c} = T\vec{\lambda}, \tag{1}$$

with $\Delta c_i = c(\vec{x}_i) - c(\vec{x}_{\mathrm{ref}})$, where $\vec{x}_1,\ldots,\vec{x}_L$ are arbitrary locations. The jth column of T: T_{ij}, $i = 1,\ldots,L$ is the model concentration with reference to the concentration at $\vec{x}_{\mathrm{ref}}$ when sampled at the same locations as $\Delta\vec{c}$ and when releasing a surface flux from region j. In estimating fluxes in an inversion, this relation is postulated to hold between observed concentrations and fluxes as well as in the model, up to a measurement error ε:

$$\Delta\vec{c}_{\mathrm{obs}} = T\vec{\lambda} + \vec{\varepsilon}, \tag{2}$$

and a flux estimate from the observations is obtained by minimizing

$$(\Delta\vec{c}_{\mathrm{obs}} - T\vec{\lambda})^t C_{\Delta\vec{c}}^{-1}(\Delta\vec{c}_{\mathrm{obs}} - T\vec{\lambda}), \tag{3}$$

with respect to the λ values (superscripts t and -1 of a matrix designate the matrix's transpose and inverse, respectively). The flux estimate from region i is $F_i = \lambda_i\varphi_i$. The role of $C_{\Delta\vec{c}}$, the covariance matrix of the errors of the observations, is to weigh the model observation discrepancies inversely to the uncertainty of the observations (when measured along the principal axes of the error covariance matrix). The solution of the minimization problem is [*Houghton et al.*, 1989]

$$\lambda = (T^t C_{\Delta\vec{c}}^{-1} T)^{-1} T^t C_{\Delta\vec{c}}^{-1}\Delta\vec{c}_{\mathrm{obs}}, \tag{4}$$

with covariance matrix of the estimates (estimate uncertainties (variances) along the diagonal and their covariation, the off-diagonal elements)

$$C_\lambda = (T^t C_{\Delta\vec{c}}^{-1} T)^{-1}. \tag{5}$$

For our envisaged applications of the method, the number of observations is of the order of 200,000, and the number of fluxes in of the order of tens. The minimization problem in our case is therefore strongly overdetermined. Note that the formalism described does not allow to consider errors stemming from biases in model transport. The same holds for errors in the spatial distributions of the surface fluxes imposed to determine the

concentration distributions in the ocean interior. These errors need to be assessed independently.

For some biogeochemical cycles and for the exchange of heat, the global air-sea exchange is known to be close to zero. It may therefore be desirable to insure from the onset that this constraint is exactly fulfilled by the flux estimates. Such a hard constraint may be included into the minimization problem with help of Lagrangian multipliers or rotations of the fluxes to the subspace within which the linear constraint is fulfilled before performing the minimization (for details of the technique see the section on constrained least squares by *Golub and Loan* [1989]).

Solutions of inverse problems, whether overdetermined or underdetermined, often exhibit unrealistically large oscillations. The reason for the oscillations may lie in insufficient data coverage (as, e.g., for the retrieval of temperature profiles from satellite observations) or in the nature of the process to be inverted (as, e.g., transport of a dissolved substance within a diffusive fluid). To avoid the large oscillations in such cases, often prior estimates $\vec{\lambda}_0$ (also virtual measuremenst or soft constraints) of the fluxes with covariance matrix C_{λ_0} are invoked. In this case, the functional

$$(\Delta\vec{c}_{\text{obs}} - T\vec{\lambda})^t C_{\Delta\vec{c}}^{-1}(\Delta\vec{c}_{\text{obs}} - T\vec{\lambda}) + (\vec{\lambda} - \vec{\lambda}_0)^t C_{\lambda_0}^{-1}(\vec{\lambda} - \vec{\lambda}_0) \quad (6)$$

is minimized with solution

$$\lambda = (C_{\lambda_0}^{-1} + T^t C_{\Delta\vec{c}}^{-1} T)^{-1}(C_{\lambda_0}^{-1}\vec{\lambda}_0 + T^t C_{\Delta\vec{c}}^{-1})\vec{c}_{\text{obs}} \quad (7)$$

and with estimate covariance

$$C_\lambda = (C_{\lambda_0}^{-1} + T^t C_{\Delta\vec{c}}^{-1} T)^{-1}. \quad (8)$$

These formulas are readily interpretable as a generalization of the formula for the combination x of two independent measurements x_1 and x_2: $x = [(1/\sigma_1^2) + (1/\sigma_2^2)]^{-1}[(x_1/\sigma_1^2) + (x_2/\sigma_2^2)]$, with $\sigma^2 = [(1/\sigma_1^2) + (1/\sigma_2^2)]^{-1}$ [*Houghton et al.*, 1989]. An algebraically equivalent form, however, is more suited for practical computation [*Houghton et al.*, 1989]. For our method, which uses models with known deficiencies for the forward predictions, the danger of the use of prior estimates is that they may interfere with these deficiences such as to produce biased estimates. Estimating quantities from data without having to refer to prior estimates is generally preferable. Fortunately, as we will demonstrate, the existing data density of the order of several 100,000 data points is sufficient to constrain fluxes from 10 to 20 regions.

Two assumptions implicit in our methodology need further discussion. First we assume that the cycle to be analyzed has been in a steady state (i.e., that the exchange fluxes have not changed) over the multicentury timescales that would be required to substantially alter the global properties that we use for our inversion. Second we assume that the ocean circulation has not changed substantially over the same period. For carbon, oxygen, and heat there is some supporting evidence from paleodata that indeed only minor fluctuations have occurred within the last few thousand years that preceded the industrial revolution. Ice core measurements of *Indermühle et al.* [1999] and *Etheridge et al.* [1996], for example, show variations in atmospheric carbon of maximally 10 ppm over the last 4000 years. In the more recent past, the last 50–100 years, the heat content of the oceans rose in parallel to global warming *Levitus et al.* [2000]. The heat flux of 0.3 W m^{-2} implied by this heat gain [*Levitus et al.*, 2000] is small compared to the current steady state heat fluxes and thus is of minor concern. The second assumption of an ocean circulation at steady state, however, has recently been challenged by *Broecker et al.* [1999]. He suggested that the deep ocean circulation oscillates with a period of 1500 years between a state of high deep water formation rates in the North Atlantic and one of high deep water formation rates around Antarctica. Broecker et al.'s hypothesis remains speculative, but we have to keep this caveat in mind when interpreting flux estimates obtained with our inverse method.

2.1. Surface Emissions

For the simulations of tracer distributions we partition the ocean surface into 15 regions (Figure 1) and use two sets of surface flux patterns (the spatial distribution of the surface flux strength within a region). The choice of flux regions is guided by the main hydrographic features of the ocean circulation and the annual mean heat fluxes estimated by *Esbensen and Kushnir* [1981]. For the 15 region partitionings, the regions are the Southern Ocean south of the Polar Front (58°S), three Southern Hemisphere subpolar regions (58°–36°S), three Southern Hemisphere temperate regions (36°–13°S), three equatorial regions (13°S–13°N), two Northern Hemisphere temperate regions (13°–36°N in the Pacific; 13°–53°N in the Atlantic), and two Northern Hemisphere subpolar and polar regions (36°–62°N in the Pacific; 53°–90°N in the Atlantic). The surface flux patterns that we employ are either spatially uniform or have the same spatial pattern as the annual mean heat flux estimated by *Esbensen and Kushnir* [1981] and thus do not vary seasonally. In the few regions where *Esbensen and Kushnir* [1981] predict both positive and negative fluxes, we used the absolute value of the flux at the ocean surface to predict tracer distributions in the ocean interior. The intent was to avoid additional tracer runs at the cost of a small estimate error. We regard the use of the *Esbensen and Kushnir* [1981] flux patterns as our standard case and use the spatially uniform fluxes to determine the sensitivity of our results to the flux patterns.

2.2. Ocean Circulation Models

We use three different variants of a three-dimensional (3-D) OGCM to simulate the tracer distributions. Our standard model has been newly developed at Princeton University on the basis of the Geophysical Fluid Dynamics Laboratory (GFDL) Modular Ocean Model (MOM) Version 3 [*Pacanowski and Griffies*, 1998]. We will refer to this model as KVLOW + AILOW [*Gnanadesikan et al.*, 2001]. It is a global seasonal model with 24 vertical layers, a zonal resolution of 4.5° and a meridional resolution of 4°. The model topography is the same as used in the coupled ocean-atmosphere model described by *Manabe and Stouffer* [1994], except the numbers of vertical layers have been doubled by simply dividing each level into two levels without further adjustments. At the surface, the ocean circulation model is forced by seasonally varying wind stress from *Hellerman and Rosenstein* [1983]. Surface temperature and salinity fields are forced with a hybrid between flux and restoring boundary conditions

$$\Delta z c_p \varrho \frac{\partial T}{\partial t} = F_{sfc}^{\text{DaSilva}} + \frac{1}{\tau}\Delta z c_p \varrho (T - T_{\text{Levitus}}), \quad (9)$$

with a restoring timescale τ of 60 days (Δz is vertical dimension of the uppermost model grid box, c_p is specific heat, ϱ is density and T is model temperature). For the flux term we use the seasonally varying heat and freshwater fluxes of the *da Silva et al.* [1994] climatology and for the restoring term the seasonally varying *Levitus et al.* [1994] sea-surface temperature and *Levitus and Boyer* [1994] salinity fields. The hybrid boundary conditions ensure that the model surface temperature field stays close to the observations. Lateral advection caused by sub-grid scale eddies is included following the parameterization of *Gent et al.* [1995], using the implementation of *Griffies* [1998]. A value of 1000 m^2 s^{-1} is used for both the coefficient of mixing along isopycnals and the coefficient of eddy induced mixing (i.e. isopycnal thickness diffusivity). The functional form of the explicit vertical diffusivities are prescribed following *Bryan and Lewis* [1979], with a value of 0.15×10^{-4} m^2 s^{-1} near the surface and kept below 0.20×10^{-4}

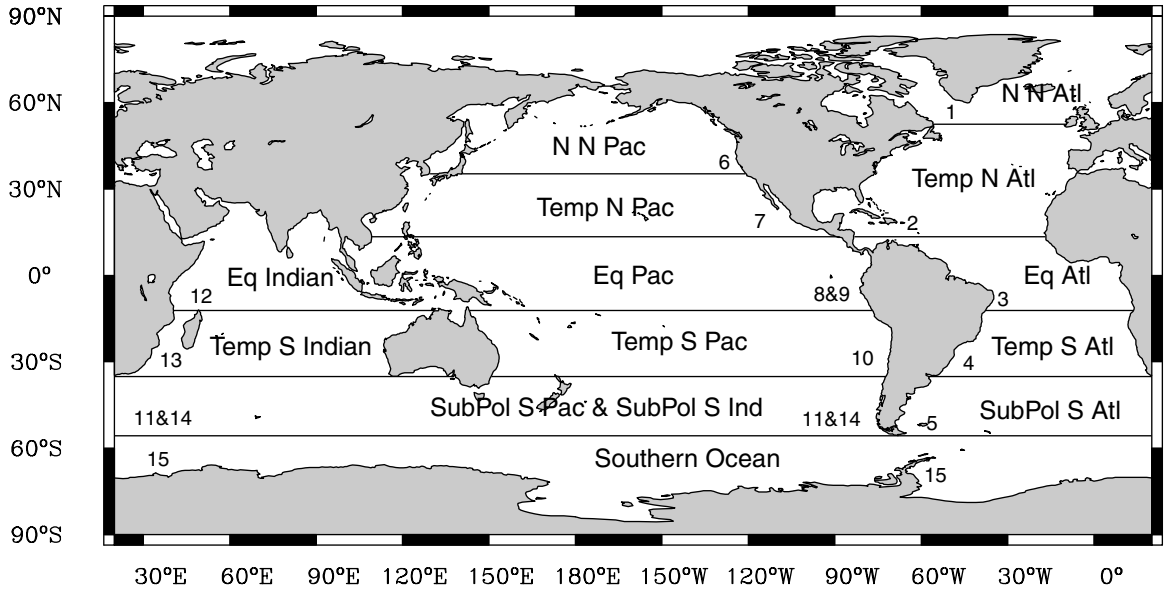

Figure 1. Map showing the partitioning of the ocean surface into 15 regions. The boundaries are at 58°S, 36°S, 13°S, 13°N, 36°N in the Pacific, and 53°N in the Atlantic. The Arctic Ocean has been combined with the polar North Atlantic.

m^2 s^{-1} throughout the thermocline, to comply with direct observations of *Ledwell et al.* [1993]. Tracers are transported online using a third order advection scheme [*Farrow and Stevens*, 1995]. No tuning has been performed with the exception of increasing bottom friction in the Bering Strait to reduce the throughflow to the observed value of 0.8 Sv [*Coachman and Aagaard*, 1988].

The simulated circulation, temperature, and salinity fields were carefully compared with direct observations [*Gnanadesikan et al.*, 2001]. The changes in resolution, physical parameterizations, and boundary conditions relative to the previous global version of the GFDL ocean model used for biogeochemical studies (Princeton Ocean Biogeochemistry Model, Version 1, POBM1) [*Sarmiento et al.*, 1995; *Murnane et al.*, 1999] leads to a significant improvement of the modeled subsurface temperature and salinity fields, in particular in the main thermocline. While POBM1 simulated temperatures were up to several degrees too warm in this depth region, this model maximally deviates by 0.5° from the observations *Gnanadesikan et al.* [2001]. The second major change is the almost complete shutdown of deep convection in the Southern Ocean as a result of the strong flattening of isopycnal surfaces induced by the Gent-McWilliams parameterization [*Gent et al.*, 1995]. This results in a very sluggish ventilation of the deep ocean from southern sources. Simulations of radiocarbon and chlorofluorocarbon reveal that this shutdown is likely too strong [*Dutay et al.*, 2001]. In order to investigate the effect of this very small deep water production in the Southern Ocean on the inversion results, we employ a variant of the KVLOW + AILOW model, where the vertical diffusivity in the Southern Ocean south of 60°S was increased to 10^{-4} m^2 s^{-1} to reduce the excessively strong stratification. This model will be referred to as KVHISOUTH + AILOW [*Gnanadesikan et al.*, 2001].

To further investigate the sensitivity of the inversion results to the employed ocean circulation model, we use a third model, which was developed by *Gnanadesikan* [1999] to study the cycling of silicon in the ocean. This model, which we will refer to as SIL, is based on the GFDL MOM code Version 2.0 [*Pacanowski*, 1996]. It has many similarities to KVLOW + AILOW: it uses the same horizontal resolution, and it uses low explicit vertical diffusivity and includes the lateral advective effect of eddies by employing the Gent-McWilliams parameterization. The main differences are that it has only 12 layers vertically, that its topography neither allows for flow through the Bering Strait nor through the Indonesian Straits, and that it is an annual mean model with restoring surface boundary conditions only. Comparison of the simulated flow pattern, temperature, salinity, natural radiocarbon, and transient tracers with observations indicate that KVLOW + AILOW and KVHISOUTH + AILOW are more successful than SIL, but these two models still exhibit several shortcomings, most significantly in the Southern Ocean and the equatorial Pacific as discussed in sections 3.4 and 4.

After spinning up the circulation models for 4000 years, the dye tracer fluxes at the ocean surface were turned on, and the model integrated for an additional 3000 years. All inversions use annual mean results from model year 7000. No depth acceleration technique was used for model spin-up.

2.3. Dye Tracer Distributions

The ability of the inversions to distinguish the origins of a given tracer release depends on how much the resulting patterns in the ocean interior differ from each other. We therefore briefly summarize the characteristics and controls of these distributions. The simulations we discuss here are those based on KVLOW + AILOW and dye release from 15 regions with a pattern that follows the heat flux estimates of *Esbensen and Kushnir* [1981].

The quasi-stationary tracer distributions obtained in the ocean fall roughly into five categories. The first three correspond to tracer release from the Atlantic, Pacific, and Indian Oceans, and the latter two correspond to tracer release from the polar North Atlantic and the Southern Ocean. A general characteristic of all the patterns (Figure 2) is the large signals close to the surface where the dye tracer is released. Besides these commonalities there are large differences in the interior of the ocean. If, as in the Atlantic basin, tracer laden water masses are readily transported to the North Atlantic convection regions, there are large signals at intermediate ocean depths. The signals in this case remain strong all along the North Atlantic Deep Water core in the Atlantic at 2000 m depth,

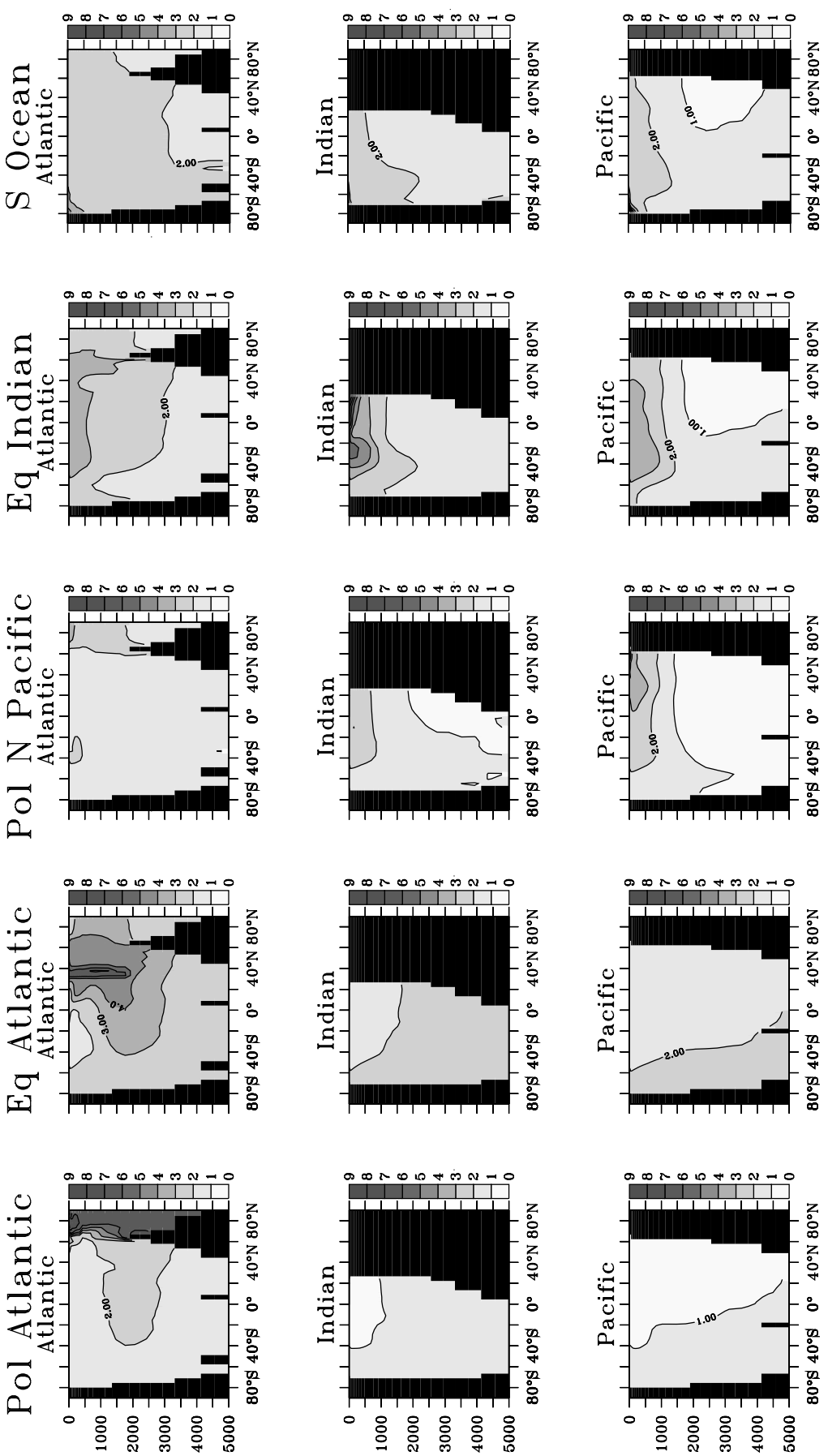

Figure 2. Zonal mean sections of basin averaged quasi-stationary dye tracer distributions (10^6 (tracer unit m^{-3}) (tracer unit m^{-2} s^{-1})$^{-1}$) when releasing tracer from five representative regions. Tracer units maybe kilograms or moles. The tracer distributions are referenced to the concentration at 3.5 km depth in the equatorial Pacific approximately at the date line. Displayed are zonal averages over the Atlantic, Indian, and Pacific Oceans. The titles like Pol Atlantic indicate the region of tracer release (see Figure 1).

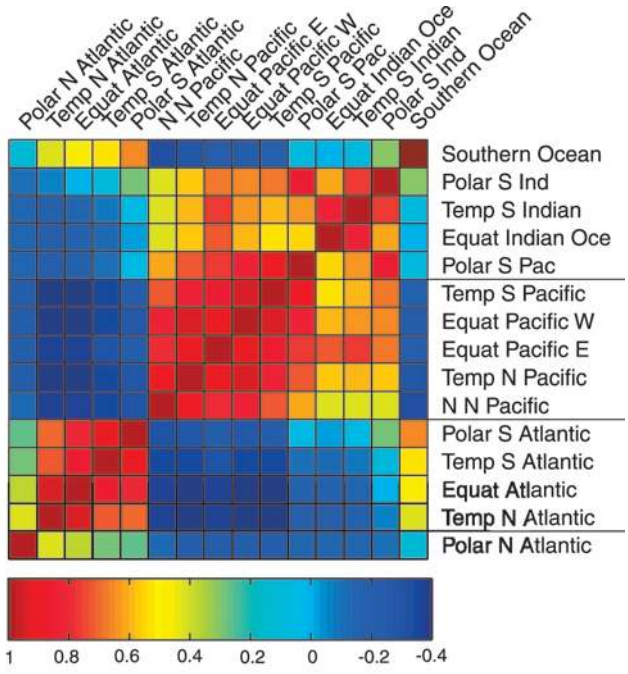

Plate 1. Correlation matrix r_{ab} of the signals obtained when releasing dye tracer from different ocean regions and when sampling at the WOCE data network.

from where they gradually diminish once they enter the circumpolar current. If tracer is released from the Pacific and Indian Oceans, however, it gets trapped in the shallow mixed and thermocline layers, and the imprint below the main thermocline is negligible. Finally, when the tracer is released from the Polar North Atlantic, there is a very strong signal over the entire water column of the Arctic Sea. By contrast, when the dye is released from the Southern Ocean region, signals are largest along the rim of Antarctica and decrease strongly with depth in the circumpolar current.

For later interpretation of the sensitivity studies of the inversions, it is helpful to look at the correlations [e.g., *Press et al.*, 1992]

$$r_{ab} = \frac{\sum_{i=1}^{n_{\text{obs}}} [c_a(\vec{x}_i) - \overline{c}_b][c_b(\vec{x}_i) - \overline{c}_b]}{\sqrt{\left(\left\{\sum_{i=1}^{n} [c_a(\vec{x}_i) - \overline{c}_b]^2\right\}\left\{\sum_{i=1}^{n_{\text{obs}}} [c_b(\vec{x}_i) - \overline{c}_b]^2\right\}\right)}} \quad (10)$$

between the signals when tracer is released from regions a and b and when sampled at all observation stations $\vec{x}_i$ (Plate 1). As expected from the characteristics of the tracer patterns, we find five types of roughly uncorrelated signals that correspond to tracer release from the two polar regions and the three main ocean basins. However, signals for dye tracer release from within each of the main basins are strongly correlated. The consequence of these correlations (i.e., the similarity of the signals) is that it is difficult to distinguish between these fluxes with an inversion. Particularly difficult regions to separate are the eastern and western equatorial Pacific as well as the subpolar South Pacific and the subpolar South Indian Ocean. For this reason we decided to consider only the sum of these estimates in this paper.

The origins of the correlations are the current geometry of the oceans (the three main basins) and the nature of the ocean circulation. Tracer released at low to middle latitudes is confined to the upper thermocline region and readily exchanged between regions by the wind driven surface circulation within each of the main ocean basin. By contrast, tracer released at high latitudes quickly enters the deep ocean and therefore leaves a very different imprint in the ocean interior. Signals for tracer release from the North Atlantic and the Southern Ocean are therefore almost uncorrelated with most of the other distributions. The dynamic reason for the correlation between the subpolar South Indian Ocean and the subpolar South Pacific as well as for the correlation between the Southern Ocean and the subpolar South Atlantic is fast tracer exchange in the Antarctic Circumpolar Current. The dependence between the signals from low to middle latitude regions of the Indian Ocean and the Pacific is caused by water exchange via the Indonesian throughflow.

The dye distributions shown in Figure 2 are also a powerful diagnostic of deficiencies of the simulation of ocean transport. First the North Atlantic Deep water plume is too shallow and extends too far southward compared with observations of, for example, salinity. It is also slightly too weak (14 Sv instead of 15–20 Sv [*Schmitz*, 1996]). The penetration of Southern Ocean water into the deep ocean when simulated with the KVLOW + AILOW model is much weaker than observed [*Dutay et al.*, 2001]. The changes in the model KVHISOUTH + AILOW from KVLOW + AILOW are designed to remedy this problem. The main difference between tracer distributions in these two models is thus for tracer release in the Southern Ocean. The penetration of tracer to the deep ocean in KVHISOUTH + AILOW is indeed closer to observations of CFCs. The main difference in transport between SIL and the KVLOW + AILOW models is the too strong upwelling of intermediate and deep ocean water in the tropics of SIL, a general deficiency of models with coarse resolution in the vertical.

2.4. Data and Data Error Covariance

For our heat flux inversions, we assembled a global high-quality data set of temperature on the basis of more than 50 cruises,

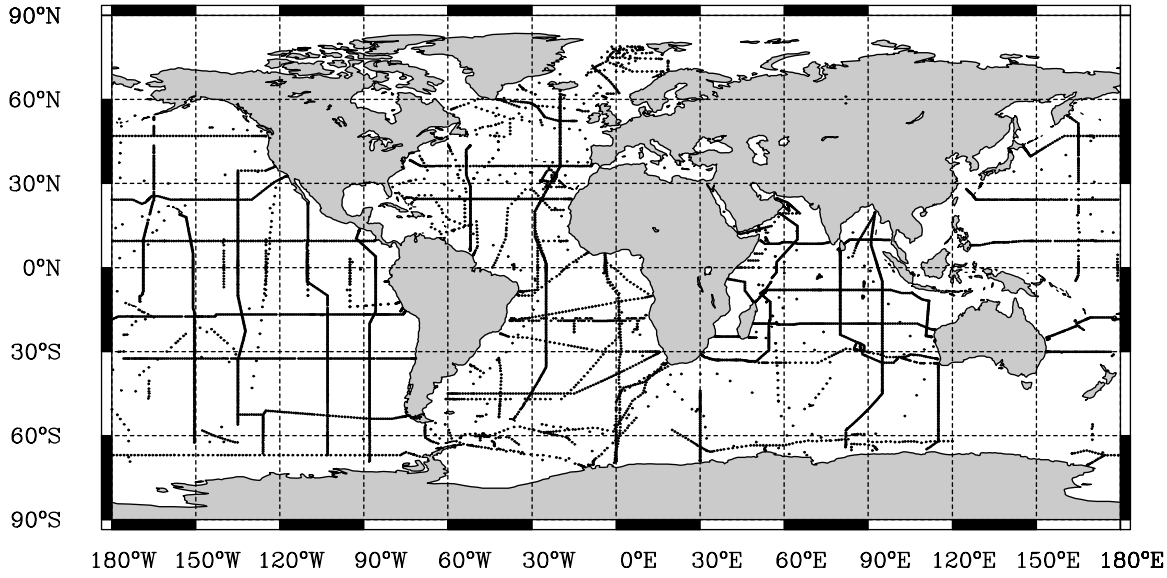

Figure 3. Map showing the station locations of the global network of profiles used in this study. See *Gruber et al.* [this issue] for further details.

predominantly gathered as part of the World Ocean Circulation Experiment (WOCE) from 1989 to 1996. This data set was augmented with some earlier data going back to the global data set obtained during the Geochemical Ocean Sections Study (GEOSECS) (1972–1978). The data set encompasses 208,000 measurements wherefrom 72% have been obtained as part of the WOCE program, 5% as part of GEOSECS and 23% during other cruises. The location of the profiles at the ocean surface are displayed in Figure 3. For a more detailed description of the data we refer to *Gruber et al.* [this issue].

As explained in section 2.3, we need to estimate the error covariance matrix to estimate flux estimate uncertainties with the standard method for linear least squares methods. For this purpose, within a given profile we determined the residuals by subtracting the data from a smoothed version of the data. The variogram indicates no correlation between the residuals. We thus use a diagonal error covariance function with a conservative value of the temperature error variance of $\sigma_T^2 = (0.2°C)^2$.

3. Robustness of Estimates

The most basic test of our method is if we succeed in recovering the heat flux imposed as a boundary condition to drive the OGCM (first bar in Figure 4) when we sample the model at the observation locations (second bar in Figure 5). Our method captures the basic global heat flux pattern; however, there are substantial differences in magnitude between the estimates and the boundary conditions particularly for the equatorial Pacific.

We may also recognize in Figure 5 a systematic pattern of trade off between the regions with similar signals (section 2.3). This concerns particularly (1) the estimates of fluxes from the temperate North Atlantic and the northern North Atlantic regions, (2) temperate North Pacific versus northern North Pacific, (3) estimates of fluxes from the Equatorial Pacific versus temperate South Pacific regions, and (4) the Southern Ocean versus polar South Atlantic.

The next few sections serve to analyze further the causes of the differences between boundary conditions and estimates and for errors in inversions in general. For this purpose we distinguish three sources for uncertainty and biases of estimates. The first source is undersampling. If sampling is too sparse, small errors in data and modeling may induce large errors in estimates. The second is modeling errors of the spatiotemporal patterns of surface fluxes used to simulate the dye distributions. Disagreement between the surface flux patterns used for the simulations and the real flux patterns may result in unrealistic pathways of the water masses and therefore again large biases. The third cause of errors is modeling errors of ocean transport.

3.1. Data Coverage

A first question before applying the method to heat or gas fluxes is if the sampling density of the observations is sufficient. To answer this question we may estimate the decrease in uncertainty of estimates caused by uncertainty in data by error propagation when increasing the sampling density and, in particular, the uncertainty when sampling at our network. If the errors for our network are large, then data coverage is likely insufficient. Note again that the errors determined by error propagation do not include any modeling error.

For the inversion scheme that resolves fluxes from 15 regions and that is based on the observations in Figure 4, we find that the flux estimate error determined by error propagation (equation (5)) is $\Delta F_i \sim 0.1$ W m^{-2}. Therefore, in sharp contrast to the inverse modeling of atmospheric transport, which is generally hampered by insufficient data coverage [*Gloor et al.*, 2000], the presently available temperature data coverage in the oceans is sufficient for the estimation of steady state heat fluxes. The remaining errors in estimations obtained with the inversion are therefore caused exclusively by errors in the modeling of oceanic tracer transport and the surface flux patterns.

To test the dependence of the biases introduced by these modeling errors on the observation network, we performed an inversion where we sampled the model simulated temperature field at every grid point rather than just at the observation locations shown in Figure 4. Surprisingly, the differences between the inversion results (Figure 5) and the boundary conditions become larger rather than smaller. What are the reasons for this unintuitive result? First, note that the annual mean *Esbensen and Kushnir* [1981] heat flux patterns according to which the dye

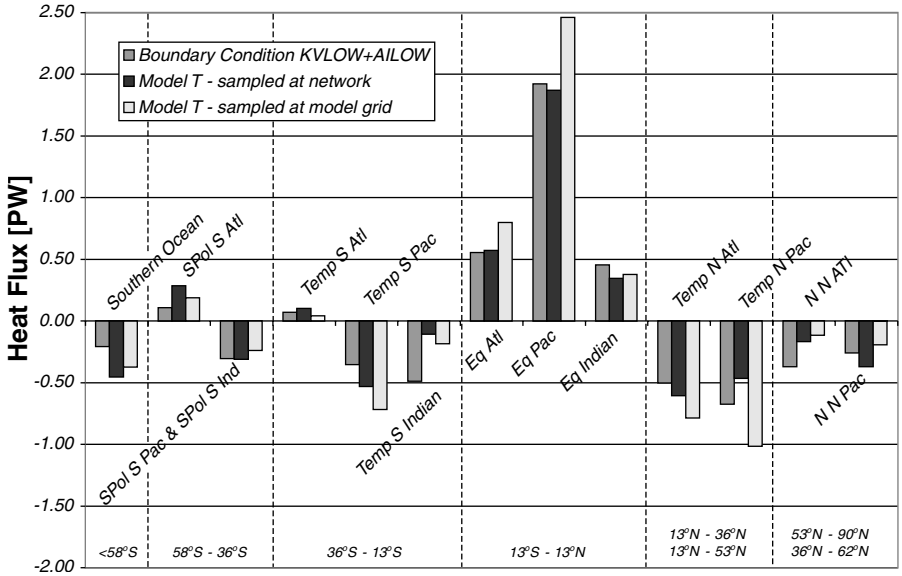

Figure 4. Comparison of annual mean heat flux estimates using model temperature of KVLOW + AILOW sampled alternatively at the model grid and the data network (Figure 3) with the heat flux applied as a model boundary condition (the sum of the *da Silva et al.* [1994] heat flux and the heat flux caused by restoring the surface temperature field to the *Levitus et al.* [1994] climatology). The flux patterns are from the heat flux climatology of *Esbensen and Kushnir* [1981].

tracers are released at the ocean surface do not agree with the flux patterns of the seasonally varying hybrid heat flux boundary conditions used to force the model (section 2.2). It is therefore not possible to represent the simulated temperature distribution exactly as a linear combination of the tracer distributions. If the observation locations happen to be located where the discrepancies between the patterns are large, biases will be large and vice versa. The effect of the discrepancies between *Esbensen and Kushnir* [1981] heat flux patterns and the model boundary condition heat flux patterns must therefore be less severe at the observation locations than when sampling at every grid box. We may confirm this claim by inspection of the difference between the model simulated temperature field T and the representation of the temperature field that is obtained when combining the tracer distributions according to the regionally integrated heat fluxes that have been applied as boundary conditions for the simulations

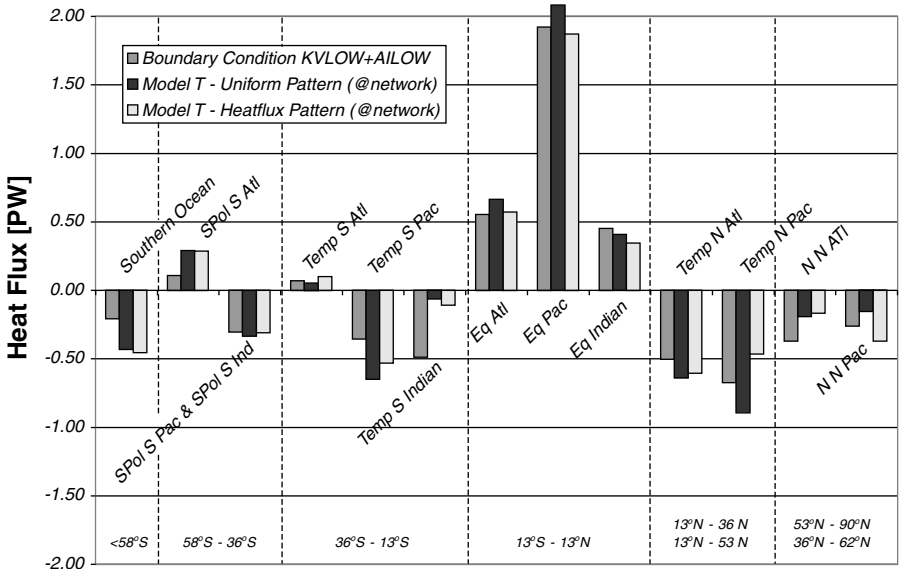

Figure 5. Comparison of annual mean heat flux estimates obtained with uniform versus *Esbensen and Kushnir* [1981] heat flux patterns and using model temperature of KVLOW + AILOW. The model in each case is sampled at the data network displayed in Figure 4.

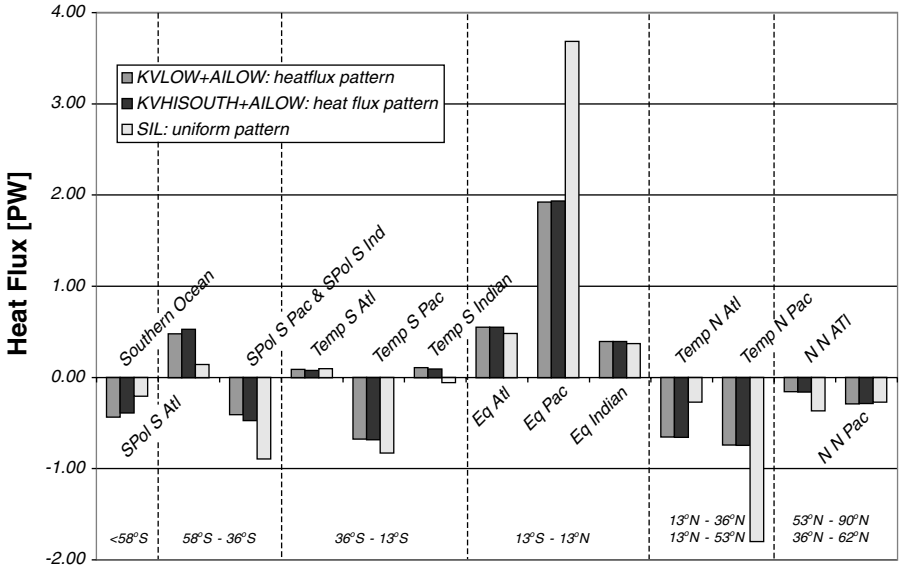

Figure 6. Comparison of annual mean heat flux estimates obtained with KVLOW + AILOW, KVHISOUTH + AILOW, and SIL inverting temperature data predominantly from WOCE. The heat flux pattern follows *Esbensen and Kushnir* [1981] for KVLOW + AILOW and KVHISOUTH + AILOW and is uniform for SIL.

(not shown). These regionally integrated heat fluxes is what the inversion would estimate if there were no mismatch between dye tracer surface patterns and the heat flux boundary conditions. At the ocean surface the differences are particularly large at the eastern and western ocean regions close to Australia and South America where observation locations are sparse. In contrast to the sampling at every model grid box, our observation network therefore is blind at these spots, and the biases of the inversion results are therefore smaller.

3.2. Sensitivity to Surface Flux Patterns

We now turn to the role played by errors in the modeling of the surface flux patterns. For this purpose we compare in Figure 5 the estimate biases when the dye tracer is released uniformly over the regions with those obtained when the dye tracer release follows the annual mean heat flux patterns as estimated by *Esbensen and Kushnir* [1981]. We find that differences between estimates obtained with uniform versus heat flux patterns are generally smaller than the difference between estimates and the model boundary conditions with the exception of the temperate North Pacific and northern North Pacific regions. We conclude that errors in the surface flux pattern are not the main contributor to the overall errors of the inversion. A second conclusion from the comparison in Figure 5 is that heat flux estimation with heat flux patterns is slightly superior to uniform flux patterns.

As an aside, we tried to see if we could resolve more details in surface flux patterns by doubling the number of regions. It turns out that there is no gain by this procedure because trade off biases (see introduction to section 3) become worse.

3.3. Sensitivity to Model Transport

We finally examine the sensitivity of the inversion estimates to the modeling of transport by comparing inversions of the temperature observations with KVLOW + AILOW, KVHISOUTH + AILOW, and SIL (Figure 6). It is immediately apparent that the inversion results are quite sensitive to the details of the ocean models. We may easily relate the differences to the specifics of the models. Consider first the differences between the two KVLOW + AILOW versions: large differences occur mainly in the partitioning of heat flux estimates between the Southern Ocean and the subpolar South Atlantic as a consequence of the increased vertical mixing in this region. One reason why estimates from these regions are so sensitive to changes in the ocean transport is the strong mixing in the circumpolar current that strongly dilutes the flux signals. Differences between the two 24 layer models (KVHISOUTH + AILOW, KVLOW + AILOW) and the 12 layer model (SIL) model inversions occur mainly in the Equatorial Pacific and temperate North Pacific. The reason for this is the too sparse vertical resolution close to the ocean surface in SIL. The model version that reproduces the observed distribution of temperature and salinity most closely is KVLOW + AILOW [*Gnanadesikan et al.*, 2001]. We therefore use the inversion results obtained with this model for comparison with heat flux estimates that are based on different methods.

3.4. Residuals: A Diagnostic of OGCM Deficiencies

Our inverse approach provides us with a powerful tool for examining the consistency between model transport and observations: the residuals $\Delta\vec{c}_{\mathrm{obs}} - \sum_{i=1}^{n} \lambda_i \Delta\vec{c}_i$ between the inverse reconstruction of the temperature field and the observations. The spatial pattern of the residuals in Plate 2 may be summarized as follows. Residuals are largest right next to the ocean surface within the shallow circulation cells associated with upwelling at the Equator and within the subduction tongues that originate from the subtropical and polar front convergence zones. One reason is that the surface fluxes used to simulate the dye tracer distributions do not have a seasonality. Other reasons are likely insufficient vertical model resolution close to the ocean surface and errors in wind-forcing and therefore misplaced wind-driven recirculation cells. Residuals at intermediate and deep levels of the oceans, albeit smaller, mirror systematic deficiencies in large-scale ocean transport. In the Atlantic and the Pacific the reconstructed temperature at middle level is too warm and in the Indian Ocean too cold. The warm bias at middle level in the Atlantic reflects the too weak and too shallow North Atlantic Deep Water

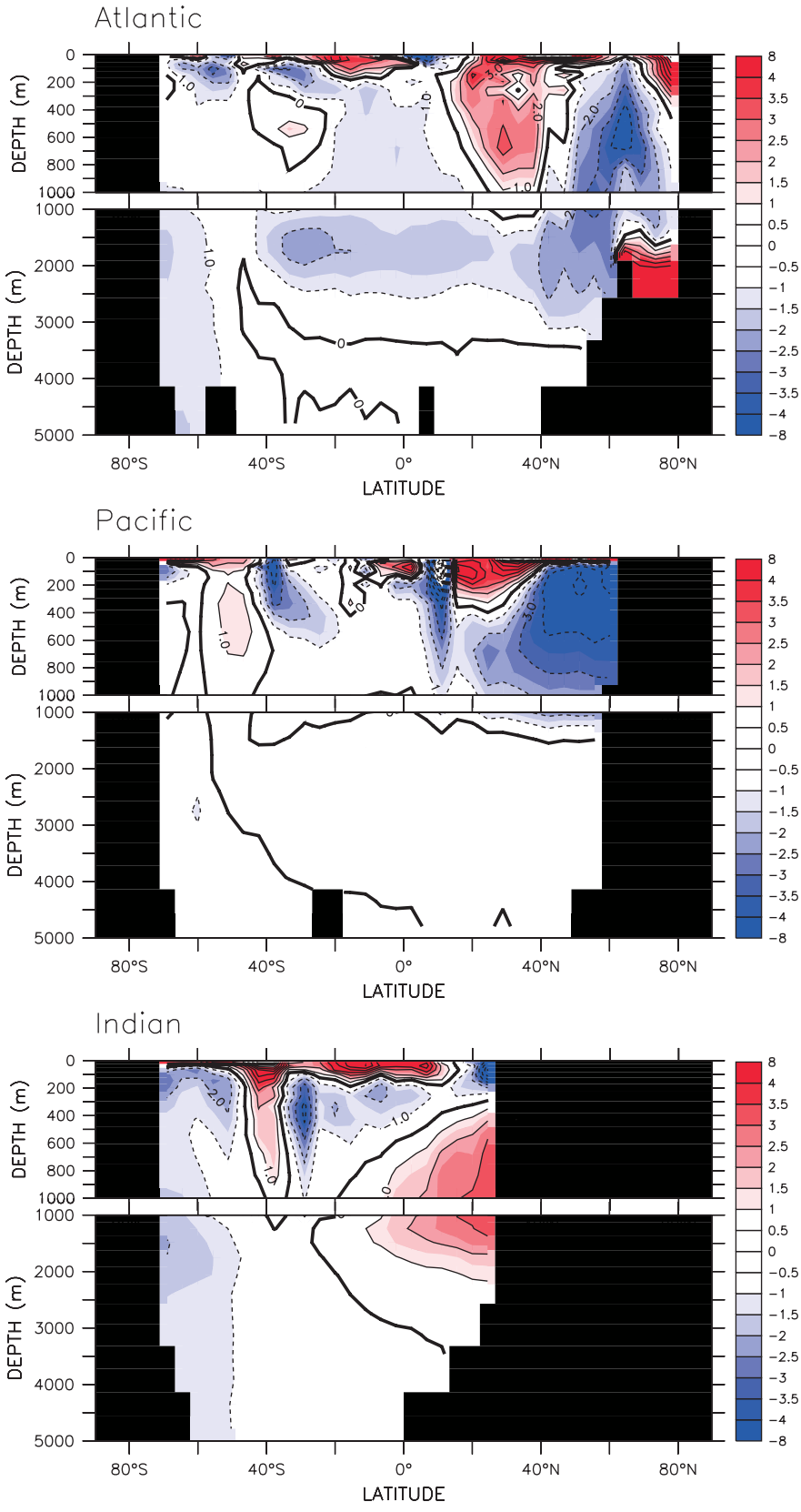

Plate 2. Zonal sections of basin averaged temperature residuals based on estimates obtained using data predominantly from WOCE and KVLOW + AILOW with *Esbensen and Kushnir* [1981] heat flux patterns. What is shown is observations minus model predictions.

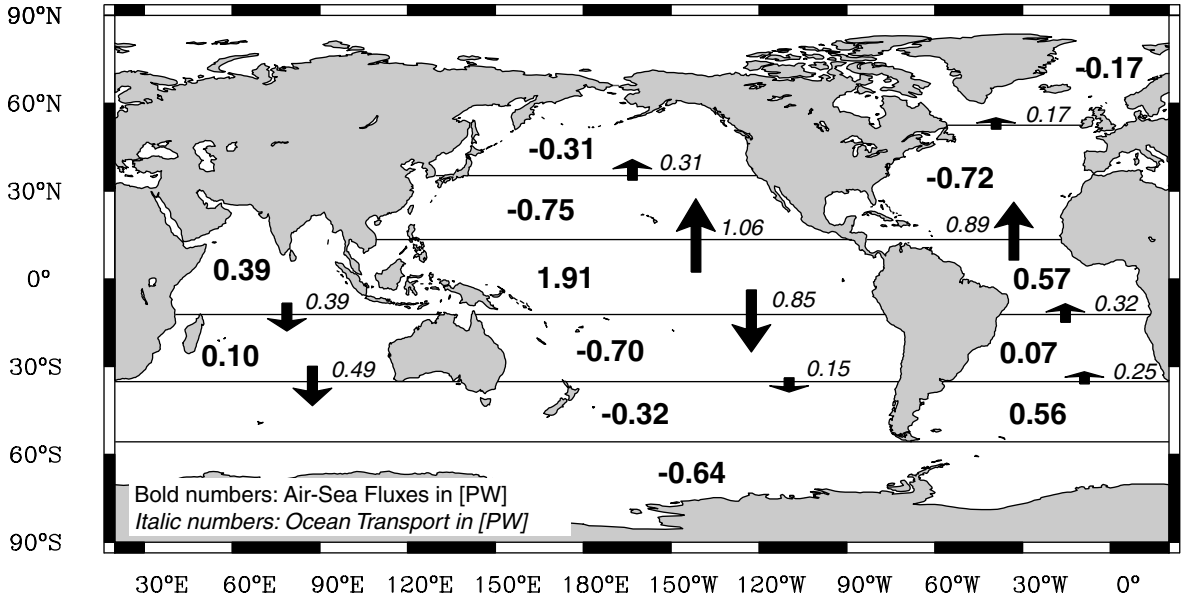

Figure 7. Annual mean heat fluxes and heat transports in the ocean interior implied by the heat flux estimates obtained using data (mainly from WOCE) and KVLOW + AILOW with *Esbensen and Kushnir*, [1981] heat flux patterns.

Circulation while the warm bias of North Pacific Intermediate Water in the Pacific maybe owing to too weak wind-forcing or too fresh waters of the Arctic Ocean. The cold bias of North Indian Intermediate Water in the Indian Ocean is likely a reflection of unrealistic renewal pathways, too sluggish deep water renewal possibly related to too weak North Atlantic Deep water formation or too weak vertical mixing and upwelling in the deep sea. Finally, the ocean regions where water temperature is reproduced the closest to observations are the Southern Ocean and all of the deep sea.

4. Heat Fluxes and Ocean Transport

Before presenting the heat flux estimates we briefly summarize the ocean heat cycle [e.g., *Peixoto and Oort*, 1992]. Five processes contribute to the energy budget of a volume V bounded by the ocean surface (in the absence of ice melting): solar shortwave radiation, R_{SW}, thermal longwave radiation, R_{LW}, latent heat loss by evaporation of water, LE, sensible heat transfer, Q_{sens}, and heat advection through the volume boundaries:

$$\frac{\partial}{\partial t}\int_V c_p \varrho \theta dv = A_{\mathrm{sfc}}(R_{\mathrm{SW}} + R_{\mathrm{LW}} + Q_{\mathrm{sens}} - \mathrm{LE}) - \int_{\partial V} c_p \varrho \theta \vec{u} d\vec{a}, \tag{11}$$

where t is time, c_p is heat capacity, ϱ is density, θ is potential temperature, dv is an infinitesimal volume element, A_{sfc} is the surface area of the volume V, $\vec{u}$ is velocity, and $d\vec{a}$ is an infinitesimal area element. The annual average energy gain from solar radiation is controlled by the Earth-Sun geometry. Large heating of the order of 220–230 W m^{-2} in the tropics (between 30°S and 30°N) gradually decreases to 80–100 W m^{-2} toward the poles. The annual average energy loss by thermal radiation reflects the gradient of the ocean temperature between the equator and the polar regions. It is of the order of 80 W m^{-2} at the equator and 50 W m^{-2} at polar regions. The driving force for the loss of sensible heat is the contrast between the ocean and atmosphere temperature. These are large along the western boundary currents and their extension to the open ocean, which transport warm water from low latitudes to high latitudes and include the Kuroshio, the East Australian current and the Gulf Stream. The contrasts are also large along narrow coastal bands within the eastern boundary currents like the Peru/Chile Current, California Current, the Canary Current, and the Benguela Current. Largest heat losses by western boundary currents in the middle to high latitudes are of the order of 50 W m^{-2}. Outside the western boundary current regions, sensible heat flux is low and of the order of 10 W m^{-2}. The driver for evaporative heat losses is the degree of saturation of the air overlying the oceans as well as the temperature of the ocean surface. They are therefore large in the tropics, of the order of 130–160 W m^{-2} and small at high latitudes, of the order of 50 W m^{-2}. Similarly to the sensible heat losses, evaporative heat losses are also strongly enhanced along the western boundary currents.

Putting all the pieces together we end up with the following qualitative picture. The oceans gain large amounts of heat of the order of 80–100 W m^{-2} within the narrow band of the upwelling regions along the equator and to a lesser degree along the eastern rims of the continents extending from the tropics to the midlatidues. The oceans lose large amounts of heat of up to 100 W m^{-2} at middle to high latitudes along the western boundary currents. The remaining midlatitude ocean regions are either weak heat sinks or sources. Note that all heat flux climatologies that we are aware of agree with this qualitative picture [*Josey et al.*, 1999; *Esbensen and Kushnir*, 1981; *da Silva et al.*, 1994]. However, the climatologies disagree considerably among each other once one starts to look at details. This concerns in particular the Southern Hemisphere high latitudes south of 50°S where flux estimates differ in magnitude and by sign.

We now first summarize our results in Figure 7. The main characteristics of the heat cycle are well captured: large heat gain in the tropics and lesser heat losses in the subtropics that almost balance when integrated over the globe (see also Table 1). The heat transports in Figure 9 implied by the surface fluxes when assuming steady state, which can be obtained from the surface heat fluxes by

Table 1. Regionally Integrated Heat Flux Estimates From WOCE Data and Comparison With the *da Silva et al.* [1994] and *Esbensen* and *Kushnir* [1981] Climatologies[a]

Region	Area, 10^{13} m^2	$\int Qda$			
		Inversion, PW	Constr. Inversion, PW	Da Silva, PW	Esbensen, PW
		Atlantic			
Northern North Atlantic	1.91	−0.16	−0.17	−0.91	−0.62
Temperate North Atlantic	3.07	−0.65	−0.72	−0.61	−0.07
Equatorial Atlantic	1.68	0.55	0.57	0.49	0.66
Temperate South Atlantic	1.48	0.09	0.07	0.10	0.31
		Pacific			
Northern North Pacific	1.89	−0.29	−0.31	−0.52	−0.43
Temperate North Pacific	3.37	−0.74	−0.75	−0.72	−0.55
Equatorial Pacific	4.96	1.90	1.91	1.16	1.16
Temperate South Pacific	3.44	−0.67	−0.70	−0.43	−0.06
		Indian			
Equatorial Indian	2.78	0.39	0.39	1.12	1.32
Temperate South Indian	2.04	0.11	0.10	−0.46	−0.12
		Southern Ocean			
Subpolar South Atlantic	1.56	0.47	0.56	0.13	0.15
Subpolar South Pacific and Subpolar South Indian	5.03	−0.41	−0.32	−0.22	−0.48
Southern Ocean	2.59	−0.43	−0.64	0.03	0.05
		Integrated			
North of 13°N	10.3	−1.83	−1.94	−2.77	−1.67
Tropics (13°S to 13°N)	9.4	2.84	2.88	2.77	3.14
South of 13°S	16.1	−0.84	−0.94	−0.86	−0.15
Global	35.8	0.17	0.00	−0.87	1.32

[a] Fluxes are positive for uptake by the oceans. Estimates obtained without and with applying a hard mass conservation constraint (indicated as "Constr. Inversion") are listed. The ocean model used is KVVHISOUTH + AILOW with the *Esbensen and Kushnir* [1981] heat flux pattern.

solving (equation (11)) for the advective transport term, furthermore reproduce well the N–S transport asymmetry between the main ocean basins: southward heat transport in the Indian Ocean, northward heat transport in the Atlantic, and nearly symmetrical heat transport in the Pacific from the tropics to the high latitudes. To obtain the heat transports we followed the usual convention that cumulates heat fluxes from North to South.

We next put our heat flux estimates based on data in perspective with independent estimates obtained using surface flux bulk parameterizations (Table 1, Figure 8), proceeding from general and global aspects to a discussion on a regional level. A general difference between the *da Silva et al.* [1994] and *Esbensen and Kushnir* [1981] estimates and ours are their large global imbalances of −0.87 and 1.32 PW, respectively. Not only our heat flux estimates, also the oxygen flux estimates [*Gruber et al.*, this issue] [this issue] almost balance fluxes globally. The reason is most likely the internal mass conserving consistency of tracer transport in the model. We may in addition impose a hard mass conservation constraint (section 2) to enforce strict mass conservation. The inversion results (third column in Table 1) prove to be fairly insensitive to this procedure, the small imbalance being mainly attributed to the Southern Ocean.

A second characteristic revealed by comparison of the estimates in Figure 10 is the good agreement between our estimates and *Esbensen and Kushnir*'s [1981] estimates over the Northern Hemisphere from 13°N northward and with *da Silva et al.*'s [1994] estimates over the Southern Hemisphere from 13°S southwards (Table 1). A third characteristic is an increasing spread between estimates going from north to south. Differences are particularly large from 36°S southward.

Guided by this observation, we start the discussion of regional heat transports in Figure 9 implied by the surface fluxes in the Northern Hemisphere and focus on the Pacific and Indian Oceans first. There is good agreement between all estimates in the Northern Hemisphere. There is also fairly good agreement between the estimates at 13°S between all three estimates when considering that our inversion tends to overestimate the 13°S southward heat flux in the Pacific at the cost of the 13°S southward heat flux in the Indian Ocean, while the sum is close to both the *Esbensen and Kushnir* [1981] and *da Silva et al.* [1994] estimates. The reason is the unrealistic modeling of the Indonesian throughflow in a coarse resolution ocean model. The Pacific-Indian Ocean passage is represented by one grid cell, and thus tracer is transported by diffusion only. For the remaining ocean in the Northern Hemisphere, the Atlantic, there is substantial disagreement. Our northern North Atlantic heat loss is very small, by far the smallest of all estimates. A likely reason is the misplaced location of North Atlantic Deep Water formation toward the South in our models. Our estimate is, however, very similar to the others when considering the more appropriate comparison of the sum of the northern North Atlantic and temperate North Atlantic heat losses. Now the *da Silva et al.* [1994] estimate is by far the largest as are the implied transports. A main reason for the better northern hemispheric agreement of fluxes between ours and *Esbensen and Kushnir* [1981] compared to *da Silva et al.*'s [1994] is the large heat loss of the latter in the northern North Atlantic.

We now turn to the Southern Hemisphere fluxes. In the Southern Hemisphere temperate regions the *Esbensen and Kushnir* [1981] heat losses are either much smaller (in the temperate South Atlantic) compared with *da Silva et al.*'s [1994] and ours or even heat gains. These discrepancies are the main reason for the much better agreement of our fluxes when integrated from 13° southward over the Southern Hemisphere compared with *da Silva et al.*'s [1994]. The biggest difference between the KVHISOUTH + AILOW heat flux estimate compared with *da Silva et al.* [1994] and *Esbensen and Kushnir* [1981] is in the Southern Ocean. There the inversion gives a heat loss of 0.43 PW (0.64 PW in the heat conserving inversion), whereas the estimates based on surface observations and bulk parameterizatons give a heat gain by the ocean of 0.03 and 0.05 PW, respectively. The Southern Ocean heat

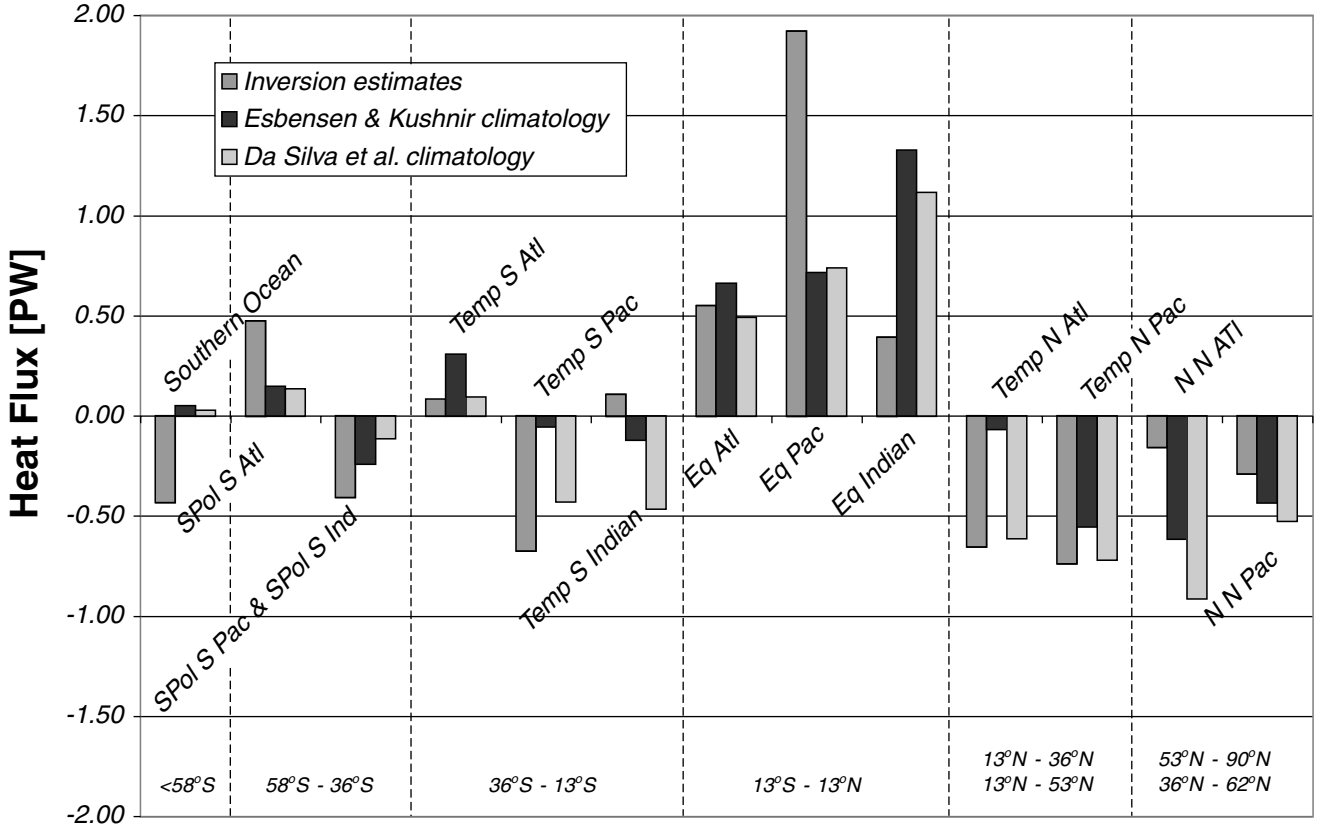

Figure 8. Comparison of annual mean heat transports obtained using data mainly from WOCE and KVLOW + AILOW with *Esbensen and Kushnir* [1981] heat flux patterns with heat transports implied by surface heat flux climatologies assuming an ocean heat cycle at steady state. The fluxes at the continental boundary of Antarctica are equal to the global imbalances.

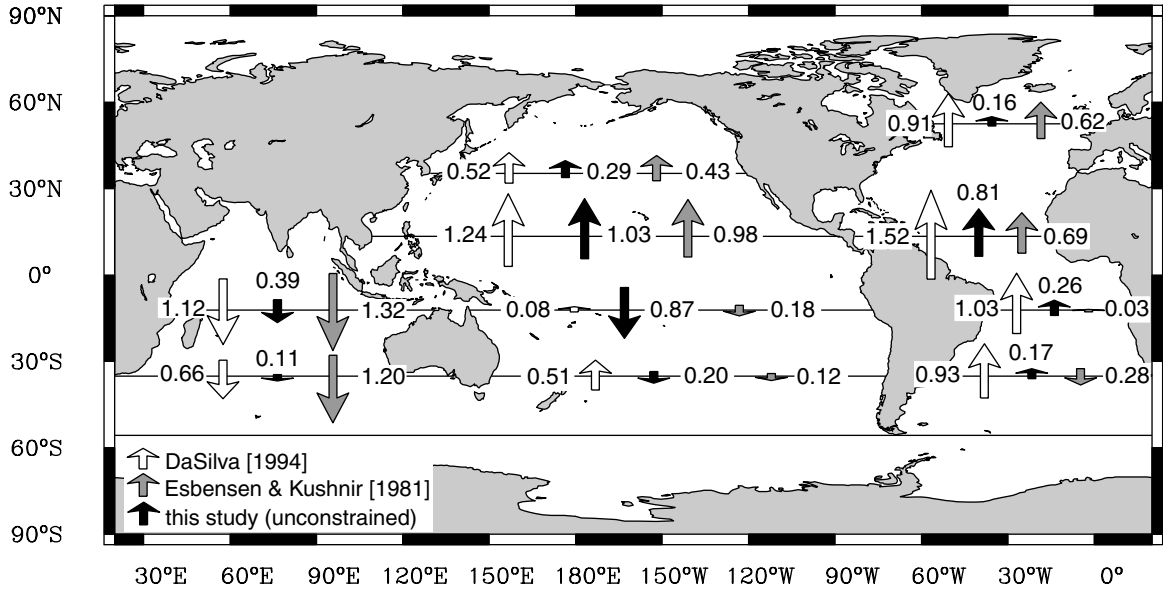

Figure 9. Comparison of annual mean heat transports obtained using data mainly from WOCE and KVLOW + AILOW with *Esbensen and Kushnir* [1981] heat flux patterns with heat transports implied by surface heat flux climatologies assuming an ocean heat cycle at steady state. The fluxes at the continental boundary of Antarctica are equal to the global imbalances.

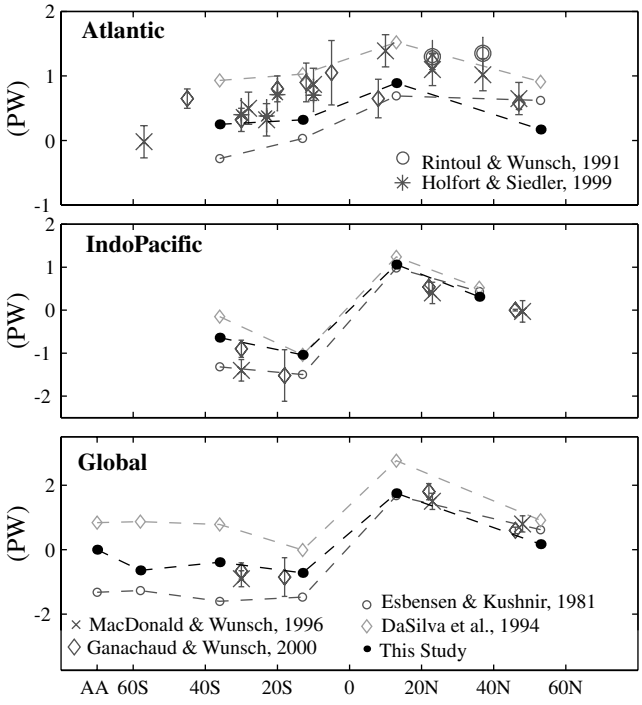

Figure 10. Comparison of annual mean heat transports in the ocean interior obtained using data mainly from the WOCE and KVLOW + AILOW applying a hard mass conservation constraint and using *Esbensen and Kushnir* [1981] heat flux patterns with published estimates based on box inverse methods and surface heat flux climatolgies. The symbol AA indicates the continental boundary of Antarctica where transports would be zero if the heat fluxes were globally in balance.

fluxes that we obtain with our inversion are extremely sensitive to the model mixing parameterization (compare Figure 6), so the uncertainty in our results is very high. The trade-off behavior between heat loss in the Southern Ocean and heat gain in the subpolar South Atlantic is not reassuring. However, we note that a wide range of other estimates of Southern Ocean heat flux give losses, just as our inversion does, with magnitudes for the region south of 60°S ranging from 0.14 to 0.54 PW [*Emig*, 1967; *Gordon*, 1981; *Hastenrath*, 1980; *Trenberth and Hurrell*, 1994]. Furthermore, our results showing a heat loss are consistent with the large gain of carbon dioxide called for by *Takahashi et al.* [1999] in his recent analysis of the air-sea flux of carbon dioxide. However, they are inconsistent with the large loss of oxygen and carbon dioxide such as those of *Keeling and Peng* [1995] and *Stephens et al.* [1998] (see *Gruber et al.* [this issue] for a further discussion of this issue). The role of the Southern Ocean in air-sea fluxes of heat as well as other properties remains highly controversial, with models showing the greatest disagreement between each other in this region [*Orr et al.*, 2001; *Sarmiento et al.*, 2000; *Dutay et al.*, 2001].

To summarize, our look at the horizontal transports shows very good agreement between transport rates in the Northern Hemisphere Pacific, reasonably good agreement in the tropical Indian Ocean and tropical Pacific, large disagreement from 35°S southward, and finally large differences in transport rates in the Atlantic mainly caused by the very large northern North Atlantic heat loss of *da Silva et al.* [1994].

We finally compare in Figure 10 our ocean heat transport estimates with the estimates of *Rintoul and Wunsch* [1991], *Macdonald and Wunsch* [1996], *Holfort and Siedler* [2000], and *Ganachaud and Wunsch* [2000], including the heat transports implied by the flux estimates of *da Silva et al.* [1994], *Esbensen and Kushnir* [1981]. The main difference between our method and the box model inverse approach of *Rintoul and Wunsch* [1991]; *Macdonald and Wunsch* [1996]; *Holfort and Siedler* [2000]; *Ganachaud and Wunsch* [2000], is that we employ an OGCM for the simulation of ocean transport instead of estimating at the same time ocean transport and surface fluxes from hydrographic data, as discussed already. In the Atlantic, with a few exceptions, the *da Silva et al.* [1994] and *Esbensen and Kushnir* [1981] transports bracket all other estimates from below and above, respectively. The reasons as just discussed are the large heat loss in the northern North Atlantic in the *da Silva et al.* [1994] climatology and the small heat loss in the Southern Hemisphere temperate region in the *Esbensen and Kushnir* [1981] climatology. In the Northern Hemisphere our estimates tend to be lower compared with the *Rintoul and Wunsch* [1991]; *Macdonald and Wunsch* [1996]; *Holfort and Siedler* [2000]; *Ganachaud and Wunsch* [2000] estimates, likely as a result of the too weak North Atlantic Deep Water Circulation. In the combined Indian and Pacific oceans as well as globally our estimates however compare very well with their estimates particulary with the most recent ones of *Ganachaud and Wunsch* [2000], who used also a data set primarily consisting of WOCE data.

5. Summary

We have examined a methodology to estimate gas exchange fluxes from ocean bulk data using an Ocean General Circulation Model by estimating heat fluxes based on new data from WOCE and comparing these with a variety of independent estimates. On the basis of a comparison with existing heat flux estimates and for a data density similar to WOCE, we conclude that our method proves to be a valuable option, provided a few caveats are kept in mind. First, the method implicitly assumes that the ocean circulation has been in a steady state over the last few hundreds of years; second, care is needed when interpreting the estimates because they are sensitive to the details of model transport; and third, it is difficult to assign estimate errors because they are largely due to model deficiencies. A possibility to further examine the robustness of the method to deficiences in transport modeling would be to use many ocean models to obtain a range of estimates. Finally, the most interesting difference of our heat flux estimates compared with heat flux climatologies is a large heat loss to the atmosphere of 0.64 PW from the Southern Ocean and a large heat gain of 0.56 PW in the Subpolar South Atlantic. These results are consistent with the large gain of carbon dioxide called for by *Takahashi et al.* [1999] in his recent analysis of the air-sea flux of carbon dioxide but inconsistent with the large loss of oxygen and carbon dioxide such as those of *Stephens et al.* [1998].

Acknowledgments. This work was supported by NASA (NAG5-3510) and the NOAA Office of Global Programs (NA56GP04039). N.G. was granted support by a Global and Climate Change fellowship from NOAA. This work was inspired by a presentation by Y. Yamanaka during his stay at Princeton University. We thank the Geophysical Fluid Dynamics Laboratory and Jerry Mahlman for providing computer time and three anonymous reviewers for helpful comments. We dedicate this paper to the memory of Tertia Hughes, who died tragically before the study was completed. referencesng agu

References

Bolin, B., and C. D. Keeling, Large-scale atmospheric mixing as deduced from the seasonal and meridional variations of carbon dioxide, *J. Geophys. Res.*, *68*, 3899–3920, 1963.

Broecker, W. S., T. H. Peng, G. Ostlund, and M. Stuiver, The distribution of bomb radiocarbon in the ocean, *J. Geophys. Res.*, *90*, 6953–6970, 1985.

Broecker, W. S., S. Sutherland, W. Smethie, T.-H. Peng, and G. Ostlund, Oceanic radiocarbon: Separation of the natural and bomb components, *Global Biogeochem. Cycles*, *9*, 263–288, 1995.

Broecker, W. S., S. Sutherland, and T. S. Peng, A Possible 20th-Century slowdown of Southern Ocean deep water formation, *Nature*, *286*, 1132–1135, 1999.

Bryan, K., and L. J. Lewis, A water mass model of the world ocean, *J. Geophys. Res.*, *84*, 2503–2517, 1979.

Coachman, L. K., and K. Aagaard, Transports through Bering Strait: Annual and interannual variability, *J. Geophys. Res.*, *93*, 15,535–15,539, 1988.

da Silva, A. M., C. C. Young, and S. Levitus, *Atlas of Surface Marine Data 1994*, vol. 1, *Algorithms and Procedures, NOAA Atlas NESDIS 6*, Natl. Oceanic and Atmos. Admin., Silver Spring, Md., 1994.

Dutay, J.-C., et al., Evaluation of ocean model ventilation with CFC-11: Comparison of 13 global ocean models, *Ocean Modell.*, in press, 2001.

Emig, M., Heat transport by ocean currents, *J. Geophys. Res.*, *72*, 2519–2529, 1967.

Enting, I. G., and J. V. Mansbridge, Latitudinal distribution of sources and sinks of atmospheric CO_2: Direct inversion of filtered data, *Tellus, Ser. B.*, *41*, 111–126, 1989.

Esbensen, S. K., and J. Kushnir, The heat budget of the global oceans: An atlas based on estimates from marine surface observations, *Rep. 29*, Clim. Res. Inst., Oreg. State Univ., Corvallis, 1981.

Etheridge, D. M., L. P. Steele, R. L. Langenfelds, R. J. Francey, J.-M. Barnola, and V. I. Morgan, Natural and anthropogenic changes in atmospheric CO_2 over the last 1000 years from air in Antarctic ice and firn, *J. Geophys. Res.*, *101*, 4115–4128, 1996.

Fan, S., M. Gloor, J. Mahlman, S. Pacala, J. Sarmiento, T. Takahashi, and P. Tans, A large terrestrial carbon sink in North America implied by atmospheric and oceanic carbon dioxide data and models, *Science*, *282*, 442–446, 1998.

Farrow, D. E., and D. P. Stevens, A new tracer advection scheme for the bryan-cox-semtner ocean model, *J. Phys. Oceanogr.*, *25*, 1731–1741, 1995.

Ganachaud, A., and C. Wunsch, Improved estimates of global ocean circulation, heat transport and mixing from new hydrographic measurements, *Nature*, *408*, 453–457, 2000.

Gent, P. R., J. Willebrand, T. J. McDougall, and J. C. McWilliams, Parameterizing eddy-induced tracer transports in ocean circulation models, *J. Phys. Oceanogr.*, *25*, 463–474, 1995.

Gloor, M., S.-M. Fan, S. W. Pacala, and J. L. Sarmiento, Optimal sampling of the atmosphere for purpose of inverse modelling — a model study, *Global Biogeochem. Cycles*, *14*, 407–428, 2000.

Gnanadesikan, A., A global model of silicon cycling: Sensitivity to eddy parameterizations and dissolution, *Global Biogeochem. Cycles*, *13*, 199–220, 1999.

Gnanadesikan, A., R. D. Slater, and J. L. Sarmiento, Oceanic vertical exchange and new production: A comparison between model results and observations, *Deep Sea Res., Part II*, in press, 2001.

Golub, G. H. and C. F. V. Loan, *Matrix Computations*, John Hopkins Univ. Press, Baltimore, Md., 1989.

Gordon, A. L., Seasonality of Southern Ocean sea ice, *J. Geophys. Res.*, *86*, 4193–4197, 1981.

Griffies, S. M., The Gent-McWilliams skew flux, *J. Phys. Oceanogr.*, *28*, 831–841, 1998.

Gruber, N., J. L. Sarmiento, and T. F. Stocker, An improved method for detecting anthropogenic CO_2 in the oceans, *Global Biogeochem. Cycles*, *10*, 809–837, 1996.

Gruber, N., E. Gloor, T. M. C. Hughes, and J. L. Sarmiento, Air-sea flux of oxygen estimated from bulk data: Implications for the marine and atmospheric oxygen cycle, *Global Biogeochem. Cycles*, this issue.

Hastenrath, S., Heat budget of tropical ocean and atmosphere, *J. Phys. Oceanogr.*, *10*, 159–170, 1980.

Hellerman, S., and M. Rosenstein, Normal monthly wind stress over the world ocean with error estimates, *J. Phys. Oceanogr.*, *13*, 1093–1104, 1983.

Holfort, J., and G. Siedler, The oceanic transports of heat and nutrients in the South Atlantic, *J. Phys. Oceanogr.*, *31* (1), 5–29, 2000.

Houghton, J. T., F. W. Taylor, and C. D. Rodgers, *Remote Sounding of Atmospheres*, Cambridge Univ. Press, New York, 1989.

Indermühle, A., et al., Holocene carbon-cycle dynamics based on CO_2 trapped in ice at Taylor Dome, Antarctica, *Nature*, *398*, 121–126, 1999.

Josey, S. A., E. C. Kent, and P. K. Taylor, New insights into the ocean heat budget closure problem from analysis of the SOC air-sea flux climatology, *J. Clim.*, *12*, 2856–2893, 1999.

Keeling, R. F., and T.-H. Peng, Transport of heat, CO_2 and O_2 by the Atlantic's thermohaline circulation, *Philos. Trans. R. Soc. London, Ser. B*, *348*, 133–142, 1995.

Keeling, C. D., S. C. Piper, and M. Heimann, A three dimensional model of atmospheric CO_2 transport based on observed winds, 4, Mean annual gradients and interannual variations, in *Aspects of Climate Variability in the Pacific and the Western Americas*, edited by D. H. Peterson, *Geophys. Monogr. Ser.*, vol. 55, pp. 305–363, AGU, Washington, D. C., 1989.

Ledwell, J. R., A. J. Watson, and C. S. Law, Evidence for slow mixing across the pycnocline from an open-ocean tracer-release experiment, *Nature*, *364*, 701–703, 1993.

Levitus, S., and T. Boyer, *World Ocean Atlas 1994*, vol. 4, *Temperature, NOAA Atlas NESDIS 3*, Natl. Oceanic and Atmos. Admin., Silver Spring, Md., 1994.

Levitus, S., R. Burgett, and T. Boyer, *World Ocean Atlas 1994*, vol. 3, *Salinity, NOAA Atlas NESDIS 3,* Natl. Oceanic and Atmos. Admin., Silver Spring, Md., 1994.

Levitus, S., J. I. Antonov, T. P. Boyer, and C. Stephens, Warming of the World Ocean, *Science*, *287*, 222–224, 2000.

Liss, P. S., and L. Merlivat, Air-sea exchange rates: Introduction and synthesis, in *The Role of Air-Sea Exchange in Geochemical Cycling*, edited by P. Buat-Ménard, pp. 113–127, D. Reidel Publishing Company, Hingham, Massachusetts, 1986.

Macdonald, A. M., and C. Wunsch, An estimate of global ocean circulation and heat fluxes, *Nature*, *382*, 436–439, 1996.

Maiss, M., and I. Levin, Global increase of SF_6 observed in the atmosphere, *Geophys. Res. Lett.*, *21*, 569–572, 1994.

Manabe, S., and R. J. Stouffer, Multiple-century response of a coupled ocean-atmosphere model to an increase of atmospheric carbon dioxide, *J. Clim.*, *7*, 5–23, 1994.

Murnane, R. J., J. L. Sarmiento, and C. LeQuéré, The spatial distribution of air-sea fluxes and the interhemispheric transport of carbon by the oceans, *Global Biogeochem. Cycles*, *13*, 287–305, 1999.

Orr, J. C., et al., Global oceanic uptake of anthropogenic carbon dioxide as predicted by four 3-D ocean models, *Global Biogeochem. Cycles*, *15*, 2001.

Pacanowski, R. C., Mom 2: Documentation, user's guide and reference manual, *GFDL Ocean Technical Report 3.1*, Geophys. Fluid Dyn. Lab., Natl. Oceanic and Atmos. Admin., Princeton, N. J., 1996.

Pacanowski, R. C., and S. M. Griffies, Mom 3, version 1: Documentation, user's guide and reference manual, *GFDL Ocean Tech. Rep. 3.4*, Geophys. Fluid Dyn. Lab., Natl. Oceanic and Atmos. Admin., Princeton, N. J., 1998.

Peixoto, J. P., and A. H. Oort, *Physics of Climate*, Am. Inst. of Phys., New York, 1992.

Press, W., S. Teukolsky, W. Vetterling, and B. Flannery, *Numerical Recipes*, Cambridge Univ. Press, 2nd ed., New York, 1992.

Rintoul, S. R., and C. Wunsch, Mass, heat, oxygen and nutrient fluxes and budgets in the North Atlantic Ocean, *Deep Sea Res.*, *38*, suppl. 1, S355–S377, 1991.

Sarmiento, J. L., R. Murnane, and C. LeQuéré, Air-sea CO_2 transfer and the carbon budget of the North Atlantic, *Philos. Trans. R. Soc. London, Ser. B*, *348*, 211–219, 1995.

Sarmiento, J. L., P. Monfray, E. Maier-Reimer, O. Aumont, R. Murnane, and J. Orr, Sea-air fluxes and carbon transport: A comparison of three ocean general circulation models, *Global Biogeochem. Cycles*, *14*, 1267–1281, 2000.

Schmitz, W. J., On the world ocean circulation: Volume II, *Tech. Rep. WHOI-96-08*, Woods Hole Oceanogr. Inst., 2nd ed., Woods Hole, Mass., 1996.

Stephens, B. B., R. F. Keeling, M. Heimann, K. D. Six, R. Murnane, and K. Caldeira, Testing global ocean carbon cycle models using measurements of atmospheric O_2 and CO_2 concentration, *Global Biogeochem. Cycles*, *12*, 213–230, 1998.

Stuiver, M., P. D. Quay, and H. G. Ostlund, Abyssal water carbon-14 distribution and the age of the world oceans, *Science*, *219*, 849–851, 1983.

Takahashi, T., R. A. Feely, R. Weiss, R. H. Wanninkhof, D. W. Chipman, S. C. Sutherland, and T. T. Takahashi, Global air-sea flux of CO_2: An estimate based on measurements of sea-air pCO_2 difference, in *Revelle Symposium: Proceedings of the National Academy of Sciences*, edited by C. D. Keeling, vol. 94, pp. 8292–8299, Am. Soc. for Microbiol., Washington, D. C., 1997.

Takahashi, T., R. H. Wanninkhof, R. F. Weiss, D. W. Chipman, N. Bates,

J. Olafsson, C. Sabine, and S. C. Sutherland, Net sea-air CO_2 flux over the global oceans: An improved estimate based on the sea-air pco_2 difference, paper presented at 2nd International Symposium, CO2 in the Oceans, Cent. Global Env. Res., Tsukuba, Jpn., 1999.

Trenberth, K. E., and J. W. Hurrell, Decadal atmosphere-ocean variations in the Pacific, *Clim. Dyn.*, *9*, 303–319, 1994.

Wanninkhof, R., Relationship between wind speed and gas exchange over the ocean, *J. Geophys. Res.*, *97*, 7373–7382, 1992.

Wanninkhof, R., and W. R. McGillis, A cubic relationship between air-sea CO_2 exchange and wind speed, *Geophys. Res. Lett.*, *26* (13), 1889–1892, 1999.

Wanninkhof, W., J. Ledwell, and J. Crusius, Gas transfer velocities on lakes measured with sulfur hexafluoride, in *Air-water mass transfer: Selected papers from the Second International Symposium on Gas Tranfer at Water Surfaces*, edited by S. C. Wilhelms and J. S. Gulliver, pp. 441–458, Am. Soc. Civil Eng., New York, 1991.

Watson, A. J., R. C. Upstill-Goddard, and P. S. Liss, Air-sea gas exchange in rough and stormy seas measured by a dual tracer technique, *Nature*, *349*, 145–147, 1991.

M. Gloor, Max-Planck Institut für Biogeochemie, Postfach 100164, Jena, D-07701 Germany. (mgloor@bgc-jena.mpg.de)

N. Gruber, Institute of Geophysics and Planetary Physics and Department of Atmospheric Sciences, 5853 Slichter Hall, University of California, Los Angeles, Los Angeles, CA 90095, USA. (ngruber@igpp.ucla.edu)

J. L. Sarmiento, Atmospheric and Oceanic Sciences Program, Princeton University, Sayre Hall, Forrestal Campus, P.O. Box CN710, Princeton, NJ 08544-0710, USA. (jls@splash.princeton.edu)

(Received May 12, 2000; revised March 20, 2001;
accepted March 28, 2001.)